Journal of Medicinal Chemistry Article

J. Med. Chem. **2009,** *52,* 6637–6648 **6637**
DOI: 10.1021/jm9008696

Stereoselective Behavior of the Functional Diltiazem Analogue 1-[(4-Chlorophenyl)sulfonyl]-2-(2-thienyl)pyrrolidine, a New L-Type Calcium Channel Blocker

Emanuele Carosati,[†] Roberta Budriesi,*[,‡] Pierfranco Ioan,*[,‡] Gabriele Cruciani,[†] Fabio Fusi,[§] Maria Frosini,[§] Simona Saponara,[§] Francesco Gasparrini,[∥] Alessia Ciogli,[∥] Claudio Villani,[∥] Philip J. Stephens,[⊥] Frank J. Devlin,[⊥] Domenico Spinelli,[#] and Alberto Chiarini[‡]

[†]*Dipartimento di Chimica, Università degli Studi di Perugia, Via Elce di Sotto 10, 06123 Perugia, Italy,* [‡]*Dipartimento di Scienze Farmaceutiche, Università degli Studi di Bologna, Via Belmeloro 6, 40126 Bologna, Italy,* [§]*Dipartimento di Neuroscienze, Università degli Studi di Siena, Via A. Moro 2, 53100 Siena, Italy,* [∥]*Dipartimento di Chimica e Tecnologie del Farmaco, Università "La Sapienza", Piazzale A. Moro 5, 00185 Roma, Italy,* [⊥]*Department of Chemistry, University of Southern California, Los Angeles, California 90089-0482, and* [#]*Dipartimento di Chimica "G. Ciamician", Università degli Studi di Bologna, Via Selmi 2, 40126 Bologna, Italy*

Received June 15, 2009

We studied the stereoselective behavior of 1-[(4-chlorophenyl)sulfonyl]-2-(2-thienyl)pyrrolidine, a recently described blocker of cardiovascular L-type calcium channels that binds to the diltiazem site. Given the stereocenter at C-2 of the pyrrolidine ring, the two enantiomers were separated by chiral HPLC and, using VCD in conjunction with DFT calculations of chiroptical properties, the absolute configuration was assigned as *R*-(+)/*S*-(−). For both forms, functional, electrophysiological, and binding properties were studied and the three-dimensional superimpositions of the two enantiomers over diltiazem were obtained in silico. The significant differences observed for the two enantiomers well agreed with the experimental data, and molecular regions were hypothesized as responsible for the cardiac stereoselectivity and vascular stereospecificity.

Introduction

The search for new chemotypes for any pharmacological target requires the high- or low-throughput analysis of large private or commercial libraries, followed by biological testing. Today an ever increasing interest exists in computational strategies for enhancing the enrichment capability of such preliminary screening, in other words for finding molecules with the desired pharmacological activity. These are usually referred to as hits. For this reason both industrial and academic research laboratories routinely use cost- and time-saving in silico approaches, such as virtual screening, to search through large chemical databases[1] with the aim of finding new chemotypes and/or to identify new chemical groups related to the desired biological activity in order to design more potent and selective molecules.

Our group is involved in the research field of L-type calcium channels (LTCCs[a]) blockers, with a special interest in the diltiazem (**1**) binding site. The synergic application of many different techniques is directed toward the discovery of new molecules with LTCC-blocking activity. In this context, we first optimized the inotropic activity of a series of thiazinooxadiazolones,[2,3] then recently developed a ligand-based virtual screening (LBVS) procedure that provided some interesting hits[2] that are structurally different from the starting compound. The *R*-(−) form of 8-(4-bromophenyl)-8-ethoxy-5-methyl-8*H*-[1,4]thiazino[3,4-*c*][1,2,4]oxadiazol-3-one (**2**, in previous papers named **5b**)[4] (Chart 1) was the reference compound used in the cited LBVS procedure.[4] It was used as reference because of its selective and relevant negative inotropic activity, enantiospecificity, and binding to the diltiazem site of LTCCs. With the LBVS only 20 molecules were selected and

Chart 1

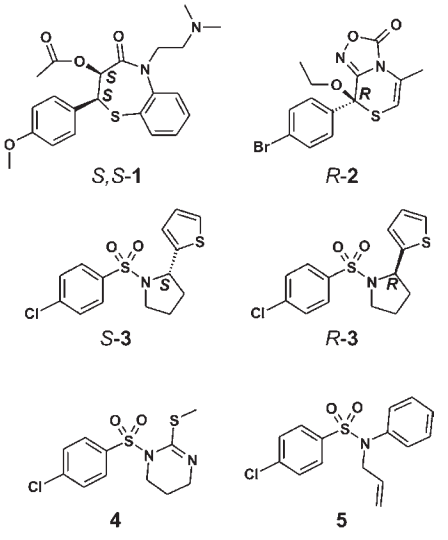

*To whom correspondence should be addressed. For R.B.: phone, +39-051-2099737; fax, +39-051-2099721; e-mail, roberta.budriesi@unibo.it. For P.I.: phone, +39-051-2099737; fax, +39-051-2099721; e-mail, pierfranco.ioan3@unibo.it.

[a]Abbreviations: AC, absolute configuration; B3PW91/TZ2P, method to calculate the vibrational circular dichroism spectra; BTZ, benzothiazepine; CD, circular dichroism; DFT, density functional theory; DTZ, diltiazem; ECD, electronic circular dichroism; FLAP, fingerprint for ligands and proteins; GPILSM, guinea-pig ileum longitudinal smooth muscle; HPLC, high performance liquid chromatography; LBVS, ligand based virtual screening; LCS, low Ca^{2+} solution; LTCC, L-type calcium channel; MIF, molecular interaction fields; OR, optical rotation; PSS, physiological salt solution; rmsd, root mean square deviation; SAR, structure−activity relationship; VCD, vibrational circular dichroism.

Published on Web 10/15/2009

Table 1. Functional Activity of Tested Compounds

	cardiac activity									
	% decrease (M ± SEM)		EC_{50} of inotropic negative activity		vasorelaxant activity			GPILSM relaxant activity		
compd	negative inotropic activity[a]	negative chronotropic activity[b]	EC_{50}[c] (μM)	95% conf lim ($\times 10^{-6}$)	activity[d] (M ± SEM)	IC_{50}[c] (μM)	95% conf lim ($\times 10^{-6}$)	activity[e] (M ± SEM)	IC_{50}[c] (μM)	95% conf lim ($\times 10^{-6}$)
1[f]	78 ± 3.5	94 ± 5.6[g]	0.79	0.70−0.85	88 ± 2.3	2.6	2.2−3.1	98 ± 1.5[h]	0.11	0.085−0.13
R-(−)-**2**	58 ± 3.4[h]	16 ± 0.8	0.07	0.04−0.08	11 ± 0.7[k]			3 ± 0.2[k]		
(*R*,*S*)-(±)-**3**	84 ± 1.6[g]	4 ± 0.2[k]	0.31	0.22−0.42	74 ± 2.1	5.62	4.46−7.08	90 ± 0.7	1.18	0.84−1.67
4	92 ± 0.9	5 ± 0.4[k]	1.33	1.04−1.70	57 ± 1.6	25.1	15.3−32.0	83 ± 2.6[i]	14.77	11.1−19.7
5	73 ± 1.4[h]	5 ± 0.3[k]	0.31	0.24−0.39	54 ± 3.1[j]	17.7	14.3−21.7	83 ± 1.7	4.32	3.65−5.11

[a] Activity: decrease in developed tension in isolated guinea pig left atrium at 10^{-5} M, expressed as percent changes from the control ($n = 4-6$). The left atria were driven at 1 Hz. The 10^{-5} M concentration gave the maximum effect for most compounds. [b] Activity: decrease in atrial rate in guinea pig spontaneously beating isolated right atria at 10^{-4} M, expressed as percent changes from the control ($n = 6-8$). Pretreatment heart rate ranged from 170 to 195 beats/min. The 10^{-4} M concentration gave the maximum effect for most compounds. [c] Calculated from log concentration−response curves (Probit analysis according to Litchfield and Wilcoxon with $n = 6-8$).[10] When the maximum effect was <50%, the EC_{50} inotropic, EC_{30} chronotropic, and IC_{50} values were not calculated. [d] Activity: percent inhibition of calcium-induced contraction in 80 mM K^+-depolarized guinea pig aortic strip at 10^{-4} M. The 10^{-4} M concentration gave the maximum effect for most compounds. [e] Percent inhibition of calcium-induced contraction in 80 mM K^+-depolarized guinea pig longitudinal smooth muscle (GPILSM) at 10^{-5} M. The 10^{-5} M concentration gave the maximum effect for most compounds. [f] $EC_{30} = 0.07$ (confidence limit 0.064−0.075). [g] At 5×10^{-6} M. [h] At 10^{-6} M. [i] At 5×10^{-5} M. [j] At 5×10^{-4} M. [k] $P < 0.05$.

biologically tested, and seven hits were found to be very promising for their LTCCs negative inotropic activity; furthermore, few vasorelaxant compounds were found as well.

On one hand, the negative inotropic activity refers to the decrease of myocardial contractility, and compounds with such activity have clinical application to decreasing the cardiac workload in conditions such as hypertrophic obstructive cardiomyopathy.[5] A vasorelaxant compound, on the other hand, is a drug that relaxes the smooth muscle in blood vessels, thus being useful in pathologies such as hypertension.[6]

Interestingly, the selective negative inotropic versus chronotropic and vasorelaxant activity, observed for the reference compound **2**, was found in many but not all screened hits. In particular, three other compounds were shown to exhibit vasorelaxant properties; in addition to (±)-1-[(4-chlorophenyl)sulfonyl]-2-(2-thienyl)pyrrolidine, ((±)-**3**, in a previous paper named as (±)-**M8**),[4] the most interesting among the three,[2] there were 1-[(4-chlorophenyl)sulfonyl]-2-(methylthio)-1,4,5,6-tetrahydropyrimidine (**4**, previously named as **M4**)[4] and *N*-allyl-4-chloro-*N*-phenylbenzenesulfonamide (**5**, previously named as **B3**).[4]

The further investigation of some of the hits found by virtual screening is inserted within our framework of analysis[7] and search for new chemotypes.[4,8] The present study was carried out to explore the chemical space around the thiazinooxadiazolone and benzothiazepine (BTZ) scaffolds[4,7] and to obtain information on variations of structural features responsible for LTCC blocking activities. In particular, these three compounds (**3**, **4**, and **5**) possess a common *p*-chlorobenzensulfonamidic scaffold that is differently substituted at the nitrogen, which for **4** is part of a six-membered ring (the tetrahydropyrimidin-1-yl residue), for **5** is bisubstituted with phenyl and allyl groups, and for (±)-**3** is part of a five-membered ring (the pyrrolidin-1-yl residue). Considering the chiral center in the pyrrolidine ring of **3**, the two enantiomers were considered separately,[9] and a stereoselective behavior was observed.

Results

Overview. For comprehensive comparison with the references **1** ((+)-*cis*-diltiazem) and *R*-(−)-**2**, the pharmacological profile of **4** and **5** was completed by measuring their effect on the longitudinal smooth muscle. For compound **3**, the two enantiomers were separated by chiral HPLC, and their absolute configurations were determined using vibrational circular dichroism (VCD) in conjunction with density functional theory (DFT) calculations of their predicted chiroptical properties. Then functional, electrophysiological, and binding properties were studied for both *R* and *S* enantiomers.

Functional Characterization and Binding Profile. The effect of compounds **4** and **5** on the longitudinal smooth muscle was measured as detailed in the Experimental Section. The functional data of compounds **4** and **5**, expressed as intrinsic activity and potency values on 1 Hz driven left and spontaneously beating right atria and in 80 mM KCl depolarized vascular and nonvascular smooth muscle, are reported in Table 1 with those of references **1** and *R*-(−)-**2** as well as of compound (±)-**3**.

Compounds (±)-**3**, **4**, and **5** revealed intrinsic negative inotropic activity without chronotropic effect. In particular, compounds (±)-**3** and **5** were equipotent, weaker than *R*-(−)-**2** but 2.5-fold more potent than **1**, while compound **4** was less effective. Concerning the activity on smooth muscles, compounds (±)-**3**, **4**, and **5** showed profiles similar to that of diltiazem, all being more potent on nonvascular than on vascular smooth muscles even if less selective than **1**. Compound (±)-**3**, which is the most potent in both tissues followed by **5** and **4**, had vasorelaxant potency 2.2 times lower than **1**, whereas compounds **4** and **5** were 9.7 and 6.8 times less potent than **1**, respectively.

Binding assays with [^{3}H]diltiazem on rat cardiomyocytes were carried out for compounds **4** and **5**, while for (±)-**3** binding data have been already published.[4] Only compound **4** displayed a weak interaction with the BTZ-binding site, producing a maximum inhibition of [^{3}H]diltiazem binding of about 50% at 100 μM (Figure 1). In contrast, compound **5** stimulated [^{3}H]diltiazem binding in a concentration-dependent fashion over the concentration range 10 nM to 100 μM. Thus, compound **5** might interact with a distinct site allosterically linked to the BTZ receptor. This hypothesis is in agreement with the stimulation profile of diltiazem binding produced by dihydropyridines and phenylalkylamines in purified porcine cardiac sarcolemmal membrane vesicles reported by Garcia et al.[11] Because of its different binding profile, compound **5** might be separately investigated in detail, and only compounds **3** and **4** would be further compared with **1**.

Determination of Absolute Configuration of Compound 3. To elucidate the biological activity of (±)-**3** and to assign the

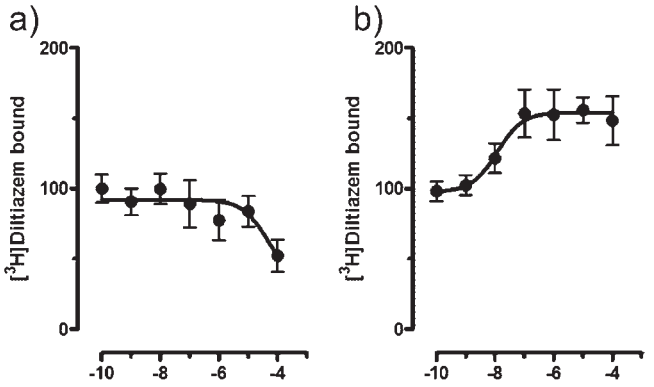

Figure 1. Effects of **4** (a) and **5** (b) on [^{3}H]diltiazem binding.

absolute configuration (AC) of its enantiomers, (±)-**3** was first separated by chiral HPLC. Then the AC of each enantiomer was determined using VCD in tandem with calculations of the predicted spectra.[12] The principle behind this powerful method for the determination of AC is determining one or more chiroptical properties of an enantiomer experimentally and comparing the spectrum/spectra with that/those predicted by DFT calculations for one AC. This technique is becoming very popular in recent years,[13−20] and it was already used to determine the AC of the above-mentioned chiral oxadiazol-3-one **2** by a concerted comparison of DFT calculations of its VCD spectrum, electronic circular dichroism (ECD) spectrum, and optical rotation (OR) to experimental VCD, ECD, and OR data.[21]

First, the pharmacologically active (±)-**3** was resolved by semipreparative enantioselective HPLC on a chiral stationary phase. Chiralpak IA was chosen as the chiral stationary phase for these purposes. The chiral selector tris-3,5-dimethylphenylcarbamate derivative of amylose immobilized on silica allows the use of a broad range of organic solvents in which the analyte is readily soluble and shows a good level of enantioselectivity and high loading ability.[22,23]

The pair of enantiomers was resolved with a selectivity value of $\alpha = 1.22$ ($k_1 = 1.33$) using hexane/isopropanol/dichloromethane (85/10/5, v/v/v) as eluent. In the semipreparative scale-up, each stereoisomer (11 mg, process yield 85%) was obtained with an enantiomeric excess of 99% (Figure 2). The elution order as monitored online by circular dichroism (CD) detection at 254 nm and off-line by polarimetric measurements on the isolated enantiomers was the (−)-enantiomer first ($[\alpha]_D^{25}$ −179.53 (*c* 0.60, CH_3CN)) and the (+)-enantiomer second ($[\alpha]_D^{25}$ +173.48 (*c* 0.64, CH_3CN)). Additional information is provided in the Experimental Section.

Then the AC of **3** was determined by comparison of experimental and predicted VCD spectra. The VCD spectra of 0.06 M $CDCl_3$ solutions of (+)-**3** and (−)-**3** were measured using cell path lengths of 236 and 546 μm; to minimize artefacts, the baselines for the spectra were the VCD spectra of racemic **3**. The resulting VCD spectrum of (+)-**3** is shown in Figure 3, together with the IR absorption spectrum of (±)-**3**. The spectra are quite dense because of the large size and conformational flexibility of **3**.

Given the conformational flexibility of **3**, its conformational analysis was also quite complicated, since there are many possible conformations. According to DFT calculations, by use of the B3PW91 functional and the TZ2P basis set, there are 10 conformations with energy values within 3

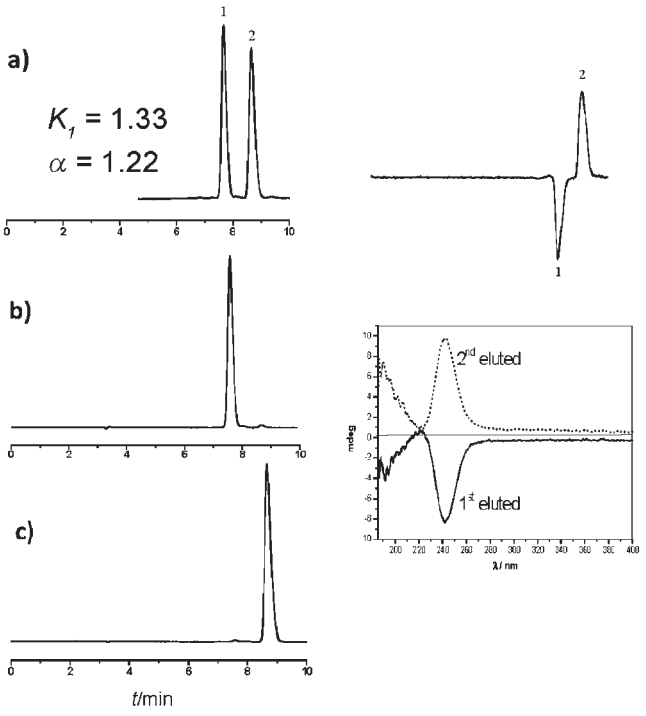

Figure 2. HPLC traces for the analysis of (a) (±)-**3**, (b) (−)-**3**, and (c) (+)-**3** monitored by UV and CD at 254 nM. Bottom right: ECD spectra of the individual enantiomers isolated by semipreparative HPLC.

kcal/mol of the lowest free-energy conformation. The free energy value of each conformation was calculated in order to evaluate the relative population of each conformation at room temperature using Boltzmann statistics. The relative free energies and the resulting room temperature populations are listed in Table 2. The prediction of the IR and VCD spectra of **3** requires calculations of the spectra of the 10 conformers and the calculation of the conformationally averaged spectra, using the calculated populations.

Finally, the B3PW91/TZ2P conformationally averaged VCD spectra of the *R* and *S* ACs of **3** were compared to the experimental VCD of (+)-**3**, as shown in Figure 4. The *R*-**3** VCD spectrum is in much better agreement with the experimental VCD spectrum than the *S*-**3** VCD spectrum. The assignment of 16 bands is indicated using the letters a−p. As a result, the AC of **3** was assigned as *R*-(+)/*S*-(−).

Determination of the LTCCs Blocking Properties of the Two Enantiomers of 3. A. Functional Study. The functional profile observed for the two enantiomers was significantly different. Data for the *S*-(−) and *R*-(+) forms of **3** are listed in Table 3 with those of (±)-**3** taken here as reference. Both enantiomers had negative inotropic activity, *R*-(+) being twice as potent as *S*-(−). Also, for the relaxant effect on guinea pig longitudinal smooth muscle, the *R*-(+) form was twice as potent as *S*-(−). In contrast, the vasorelaxant property was uniquely shown by *S*-(−)-**3**, with a potency comparable to that of (±)-**3**.

Finally, for comprehensive comparison with the three above-mentioned compounds, the pharmacological profiles of the enantiomers of **3** are graphically shown in Figure 5; (±)-**3**, **4**, and **5** had relaxant properties in guinea pig aortic strips (orange bars) and ileum longitudinal smooth muscle (fuchsia-colored bars) while showing the same selectivity profile. For all three, the inotropic activity (blue bars) was

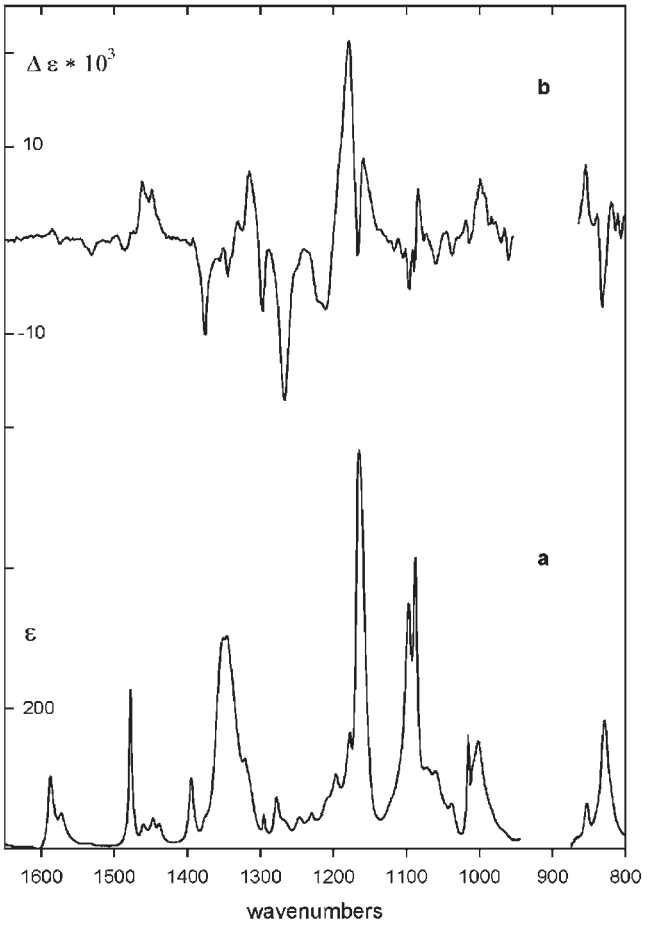

Figure 3. (a) IR absorption spectrum of racemic **3** in $CDCl_3$: 0.05 M, path length 546 μm. (b) Half-difference, $^1/_2[\Delta\varepsilon(+) - \Delta\varepsilon(-)]$, VCD spectrum of **3** in $CDCl_3$: 0.06 M. For the frequency ranges 1650−1479, 1431−1390, 1321−1200, 1072−955, and 852−800 cm^{-1} the VCD was measured with a 546 μm path length cell. For the frequency ranges 1479−1431, 1390−1321, 1200−1072, and 864−852 cm^{-1} the VCD was measured with a 236 μm path length cell.

Table 2. B3PW91/TZ2P Conformations, Free Energy Differences, and Populations of **3**

conformer	$\triangle G$ (kcal)	P (%)[a]
a	0.00	31.1
b	0.22	21.5
c	0.49	13.6
d	0.65	10.4
e	0.70	9.6
f	0.76	8.6
g	1.43	2.8
h	1.75	1.6
i	2.39	0.6
j	2.79	0.3

[a] Populations based on G values; T = 298 K.

the main effect, with the same potency registered for **5** and (±)-**3**. The latter was also the most potent compound concerning the relaxant properties on both aorta and ileum. In particular, while the negative inotropic effect was common to both enantiomers, the vascular action of **3** was only observed with the *S*-(−) form.

Finally, for comprehensive comparison, the potencies of all tested compounds on left driven atria, spontaneous beating right atria, K^+-depolarized aortic strips, and guinea pig ileum logitudinal smooth muscle (GPILSM) are graphically

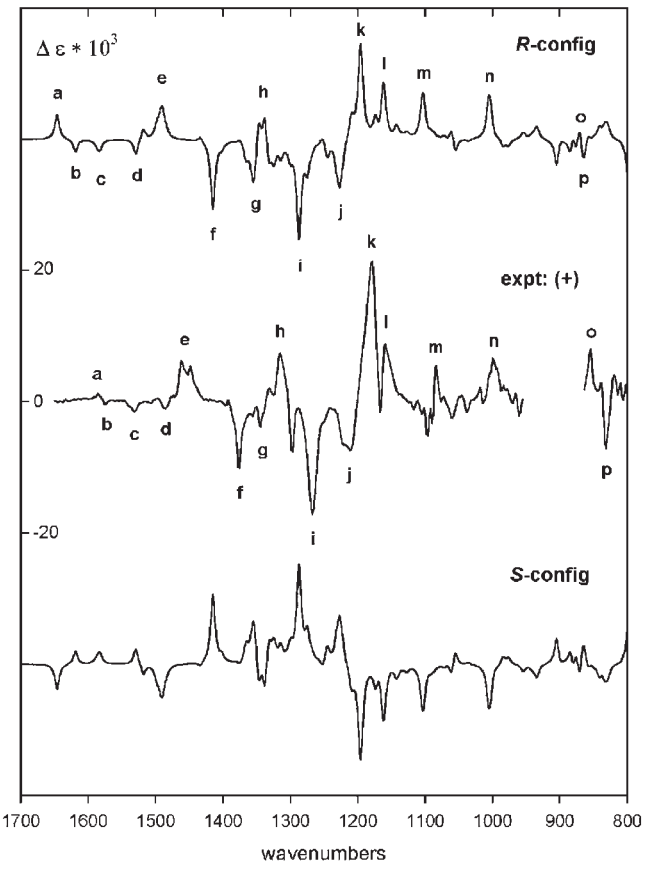

Figure 4. Comparison of the conformationally averaged B3PW91/TZ2P VCD spectra of the *R* and *S* configurations of **3** to the experimental VCD spectrum of (+)-**3**. The peaks used to assign the AC are labeled a−p.

shown in Figure 5. Diltiazem (**1**) was the less selective compound because of its activity in all tissues; conversely, *R*-(−)-**2** was the most selective one, since it showed only a negative inotropic activity. Compounds (±)-**3** and **4** had the same biological profile, similar to that of diltiazem although they lacked of chronotropic activity (green bar). Finally, it is evident in the figure that the profiles of the two enantiomers of **3** are different, with *S*-(−)-**3** being responsible for the vasorelaxant activity (orange bar) found in the racemate (±)-**3**.

B. Binding Study. Binding assays were carried out in rat cardiomyocytes to establish the binding site of the two enantiomers of **3**. [^{3}H]Diltiazem (5 nM) was incubated with increasing concentrations (0.01 nM to 100 μM) of the compounds as described in the Experimental Section.

As reported in Figure 6, *S*-(−)-**3** and *R*-(+)-**3** interacted with the BTZ-binding site, producing a reproducible inhibition of [^{3}H]diltiazem binding that reached the maximum of about 50% already at 1 μM. The findings presented in this study strongly suggest that both enantiomers of **3** equally inhibited LTCCs activity by interacting at the BTZ-binding site in the cardiac α_1 subunit of the LTCCs.

C. Electrophysiological Study. In addition, the effect of (±)-**3**, *S*-(−)-**3**, and *R*-(+)-**3** on L-type barium currents [$I_{Ba(L)}$] recorded in vascular myocytes was assessed in order to provide direct evidence of their calcium antagonistic activity. The racemic mixture of **3** and both enantiomers individually inhibited peak $I_{Ba(L)}$ in a concentration-dependent manner, with IC_{50} values of 23.5 ± 2.0 μM ((±)-**3**,

Table 3. Functional Activity of Tested Compounds

	cardiac activity									
	% decrease (M ± SEM)		EC_{50} of inotropic negative activity		vasorelaxant activity			GPILSM relaxant activity		
compd	negative inotropic activity[a]	negative chronotropic activity[b]	EC_{50}[c] (μM)	95% conf lim ($\times 10^{-6}$)	activity[d] (M ± SEM)	IC_{50}[c] (μM)	95% conf lim ($\times 10^{-6}$)	activity[e] (M ± SEM)	IC_{50}[c] (μM)	95% conf lim ($\times 10^{-6}$)
(±)-**3**	84 ± 1.6	4 ± 0.2[h]	0.31	0.22−0.42	74 ± 2.1	5.62	4.46−7.08	90 ± 0.7[f]	1.18	0.84−1.67
S-(−)-**3**	96 ± 1.7[f]	7 ± 0.3[h]	0.45	0.35−0.64	83 ± 4.5	5.16	3.33−6.99	69 ± 4.7	2.06	1.68−5.53
R-(+)-**3**	98 ± 1.1[g]	10 ± 0.7[h]	0.23	0.13−0.31	24 ± 2.3			94 ± 1.1	1.07	0.88−1.29

[a] Activity: decrease in developed tension in isolated guinea pig left atrium at 5×10^{-6} M, expressed as percent changes from the control ($n = 4-6$). The left atria were driven at 1 Hz. The 5×10^{-6} M concentration gave the maximum effect for most compounds. [b] Activity: decrease in atrial rate in guinea pig spontaneously beating isolated right atria at 5×10^{-5} M, expressed as percent changes from the control ($n = 6-8$). Pretreatment heart rate ranged from 170 to 195 beats/min. The 5×10^{-5} M concentration gave the maximum effect for most compounds. [c] Calculated from log concentration−response curves (Probit analysis according to Litchfield and Wilcoxon with $n = 6-8$).[10] When the maximum effect was <50%, the IC_{50} value was not calculated. [d] Activity: percent inhibition of calcium-induced contraction in 80 mM K^+-depolarized guinea pig aortic strip at 10^{-4} M. The 10^{-4} M concentration gave the maximum effect for most compounds. [e] Percent inhibition of calcium-induced contraction in 80 mM K^+-depolarized GPILSM at 5×10^{-6} M. The 5×10^{-6} M concentration gave the maximum effect for most compounds. [f] At 10^{-5} M. [g] At 10^{-4} M. [h] $P < 0.05$.

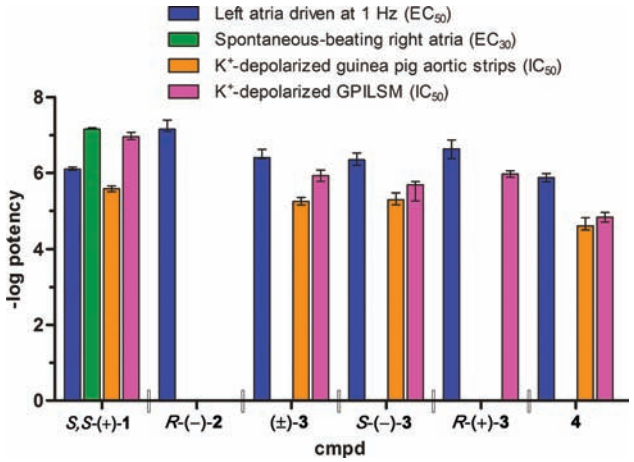

Figure 5. Negative inotropic and negative chronotropic potencies reported together with relaxant potency in 80 mM K^+-depolarized guinea pig aortic strips and ileum longitudinal smooth muscle (GPILSM) reported for the reference compounds **1** and *R*-(−)-**2**, for (±)-**3** and its *S*-(−) and *R*-(+) enantiomers, and for compound **4**.

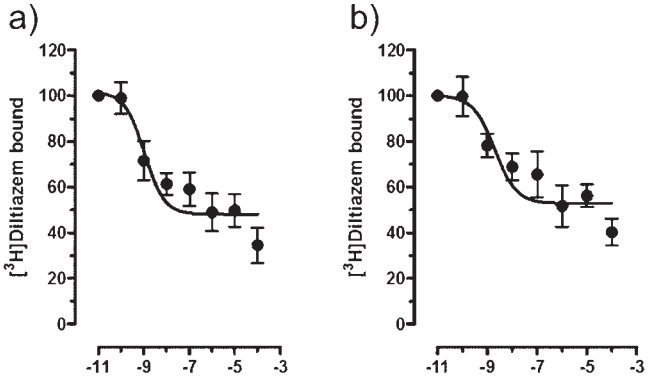

Figure 6. Binding curves for the (a) *S*-(−) and (b) *R*-(+) enantiomers of **3**.

$n = 5$), 22.2 ± 5.1 μM (*S*-(−)-**3**, $n = 4$), and 27.1 ± 8.5 μM (*R*-(+)-**3**, $n = 3$). Hence, comparable profiles for the two enantiomers and the racemic mixture emerged from this study (Figure 7).

D. Molecular Modeling Study. One of the main focuses of in silico procedures applied to drug discovery processes is to provide hypotheses for understanding which molecular

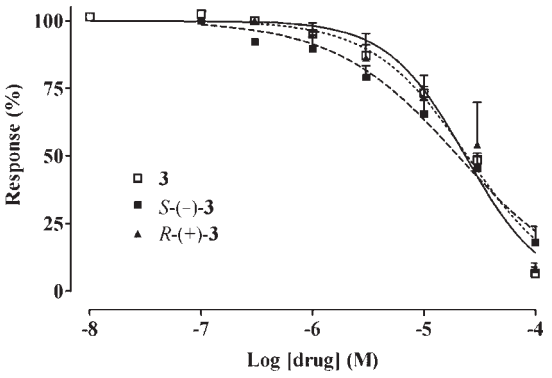

Figure 7. Effects of **3** and its enantiomers on $I_{Ba(L)}$ (5 mM Ba^{2+}, 0 mV, $V_h = -80$ mV). Each point is the mean ± SEM ($n = 4-7$). Where error bars are not shown, these are covered by the point itself.

features are important or detrimental for biological activity. Thus, a common 3D-orientation was searched for **1**, **3**, and **4** with a molecular modeling study by means of the program FLAP,[24] which is a recently developed algorithm suited to describe ligands on the basis of a common reference framework. Compound **1** was taken as reference ("template molecule"), whereas the *R*- and *S*-enantiomers of **3** and compound **4** constituted the so-called ligand molecules. Their best-possible FLAP-based orientations with respect to **1** were selected and are discussed in the next section in comparison with the experimental data. It is noteworthy that the final aim of this ligand-based application was not to claim for the compounds presented here a definitive orientation within the LTCC diltiazem binding site but to discuss one of their possible orientations with respect to **1** in order to facilitate the understanding of the relationship between molecular structure and experimental data. For a better comprehension of the 3D-superimpositions obtained, the core concepts of the program FLAP are described below while more details are given in the Experimental Section.

The program FLAP aligns two molecules one over the other and quantifies the similarity between them. The "ligand molecule" is aligned over the "template molecule", which is the reference, on the basis of their pharmacophores. A FLAP pharmacophore is a combination of four hotspots (molecular atoms): each pharmacophore of the "ligand" is searched over the "template" pharmacophores. For each match, which is obtained when four hotspots of the "ligand" molecule are found to fit over four hotspots of the

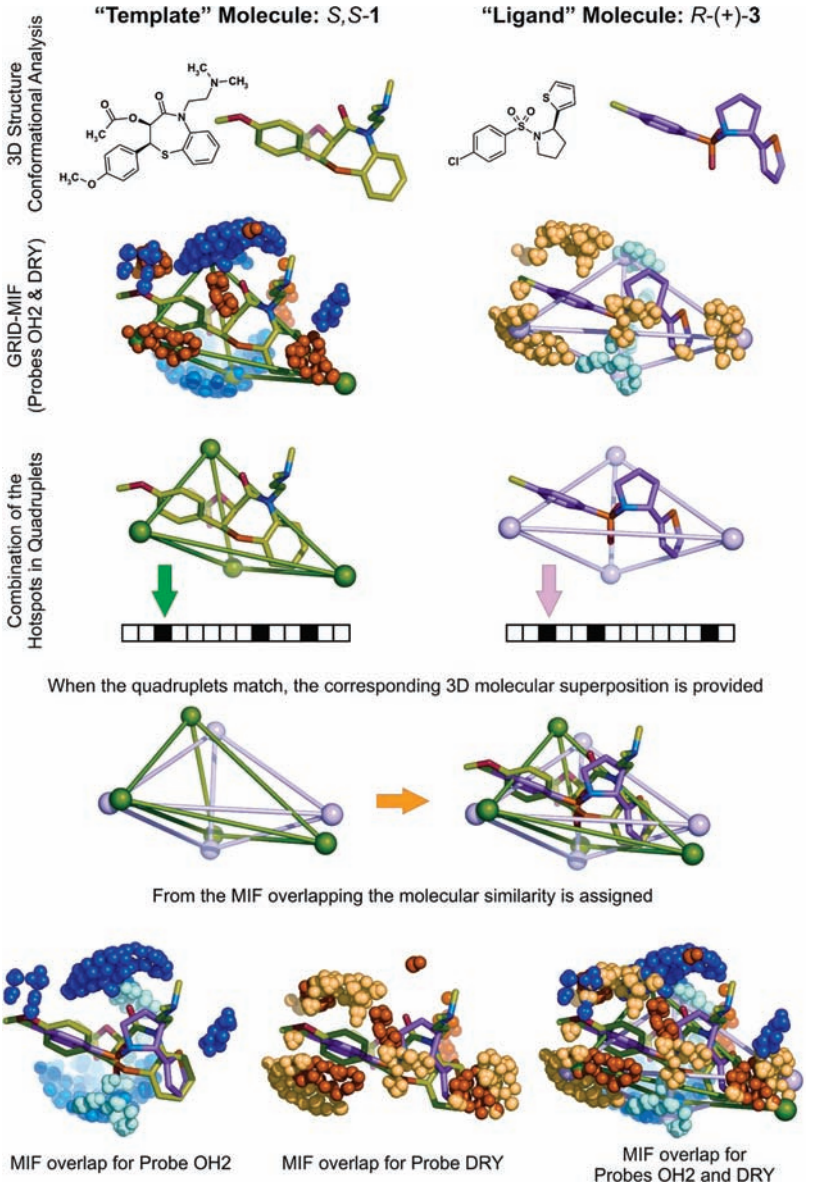

Figure 8. Scheme for the FLAP procedure that compares the "ligand" molecule *R*-(+)-**3** with the "template" molecule **1**. Nitrogen atoms are represented in blue, oxygen atoms in red, sulfur atoms in orange. Carbon atoms of **1** and *R*-(+)-**3** are differently colored (**1** = green, *R*-(+)-**3** = magenta). Hydrogen atoms are not reported for clarity. Nodes of the GRID MIF, reported at the energy level of −3.5 kcal/mol for the probe OH2 and −0.8 kcal/mol for the probe DRY, are differently colored: orange (DRY) and blue (OH2) for **1** and yellow (DRY) and cyan (OH2) for *R*-(+)-**3**. One match between two quadruplets of hotspots is reported as example. The figure was prepared using PyMol.[26]

"template", a potentially favorable superimposition is detected. This iterative process continues until all the "template" pharmacophores are combined in all possible ways with all the "ligand" pharmacophores. Each time, a score associated with the 3D-superimposition of the two molecules and with their common pharmacophores quantifies the 3D similarity. At the end of the process, only the best score obtained, which corresponds to the best superimposition of each "ligand" to the "template", is used to assess the 3D-similarity between the two molecules.

The FLAP 3D-similarity is an estimation of how the molecular interaction fields (MIF) calculated for the two molecules with the GRID force field[25] are intersected. The MIF encode into energy values the information of hydrophobic and hydrogen bonding interactions of the molecule with a virtual receptor that is schematized by the GRID probes. The best intersection of the MIF of two molecules represents the interaction with a virtual receptor that the two molecules potentially have in common.

The non-negligible flexibility of the channel and of its ligands would affect any computational study of the channel−ligand interaction, and for the same compound several possible orientations within the channel could be hypothesized. Therefore, in this study a conformational sampling guaranteed an adequate treatment of molecular flexibility. For the "template" **1** the conformational analysis was carried out on-the-fly by FLAP, producing 10 different conformations and repeating for each conformation the entire alignment procedure. Also, "ligand" molecules were subjected to a fast conformational analysis. Since the FLAP method has been created for virtual screening projects in order to run over libraries of thousands of compounds, the conformational analysis of FLAP was carried out on-the-fly to span reasonably the conformational space, a reasonable number

of conformations (up to 100) were generated for each "ligand molecule", and each conformer was treated individually. At the end of the process, only the best superimposition of each "ligand" to the "template" was memorized. A flowchart of the procedure is schematized in Figure 8.

Discussion

To date, the absence of crystallographic structures of calcium channels is likely responsible for the prevalence of ligand-based versus structure-based studies. In particular, the BTZ-binding site of LTCCs is the least characterized. Only recently, Tikhonov and Zhorov[27] have published a homology model of the pore-forming subunit (α_1) of LTCC, using ligand-docking computational experiments to elaborate a 3D model of the BTZ binding site. Their model, rationalizing various experimental observations reported in the literature,[28,29] proposes two binding modes for BTZs depending on the number of calcium ions in the selectivity-filter region. In one mode, the ammonium group of BTZ is attracted to the outer pore; this binding mode would prevail when the negative charges at the selectivity-filter glutamates in the outer pore are not compensated by calcium ions. In the other mode, the carbonyl oxygen of BTZ could directly interact with a calcium ion chelated by selectivity-filter glutamates. This binding mode would prevail when the negative charges in the selectivity-filter glutamates are instead neutralized by calcium ions. In this case, the ammonium group is not directly involved. Then for molecules without such an ammonium group a similar binding mode could be hypothesized as well.

Given the binding profiles reported above for the *R*-(+) and *S*-(−) enantiomers of **3** and for compound **4** and given the common vasorelaxant properties of **1**, (±)-**3**, and **4**, it would be interesting to provide binding mode hypotheses for *R*-(+)-**3**, *S*-(−)-**3**, and **4** in comparison with **1**. What makes it more interesting is that compounds **3** and **4** possess neither the ammonium group of **1** nor an alternative basic group with pK_a in the range of diltiazem structural analogues, i.e., 7−9.

In order to hypothesize the binding orientations, one might use the 3D-superimpositions obtained with FLAP for **4**, *R*-(+)-**3**, and *S*-(−)-**3** over **1**, reported in Figure 9. In particular, it is worth investigating the "driving motifs" of such molecular superimpositions; many polar oxygen atoms (red atoms in Figure 9) and polar groups lie in a central polar region, while a common orientation of the *p*-substituted phenyl rings can be noted for all the compounds. In particular, the 4-chlorophenyl ring of **4** is twisted when compared to the other corresponding phenyl rings and also the sulfonyl group of the sulfonamides is differently oriented for **4** with respect to *R*-(+)-**3** and *S*-(−)-**3**.

A better understanding could arise from analyzing the hydrophilic MIF in Figure 8. Two large regions are evident, which are generated by the oxygen atoms of the carboxylate group and by the carbonyl oxygen from the thiazepine moiety of **1** (blue MIF in Figure 8) and by the oxygen atoms of the sulfonyl group of *R*-(+)-**3** (cyan MIF in Figure 8). As described above, the molecular superimposition proposed is the result of the best MIF intersection for the ligand and template molecules. Thus, for both enantiomers of **3**, the sulfonyl group is aligned to the carboxylate of **1** (see Figure 9) whereas for compound **4** the best compromise of molecular shape fitted over **1** and MIF alignment (over the MIF of **1**) is obtained for the orientation proposed in Figure 9,

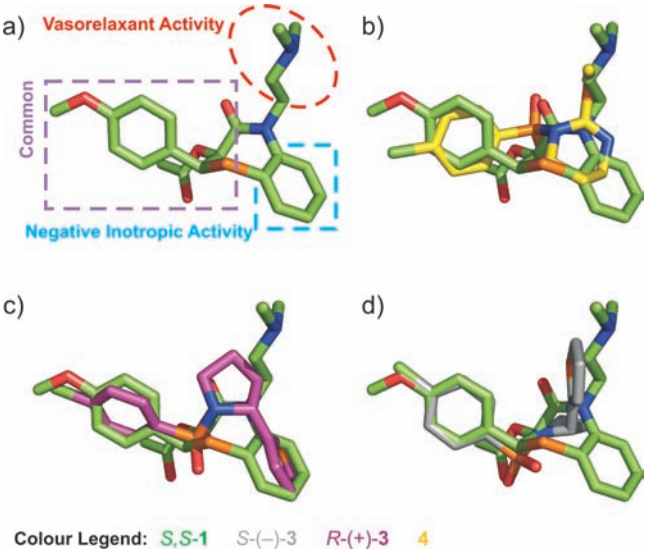

Figure 9. 3D-Superimpositions over **1** (a) obtained for **4** (b), *R*-(+)-**3** (c), and *S*-(−)-**3** (d) with the program FLAP. The figure was prepared using PyMol.[26]

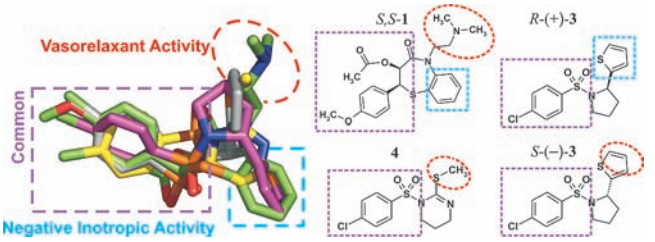

Figure 10. Chemical features hypothesized as responsible for the modulation of negative inotropic activity (highlighted in cyan squares), for vasorelaxant effect (red circles), and for both effects (purple). The 3D-superimpositions are also reported. The figure was prepared using PyMol.[26]

with the sulfonyl group aligned over the carbonyl oxygen of the thiazepine ring and the *p*-substituted phenyl ring slightly twisted. The lower inotropic and vasorelaxant activities of **4** as well as its low affinity toward the diltiazem binding site could be related to this "less precise alignment". The tetrahydropyrimidine ring, aligned over the thiazepine moiety, forces the methylmercapto group to lie over the *N*,*N*-dimethylaminoethyl side chain of **1**. Also the 2-thienyl group of *S*-(−)-**3** lies over the hydrophobic side chain of **1**, while for *R*-(+)-**3** the same ring is better aligned over the benzo-fused ring of **1**. These differences could help to rationalize the stereoselective behavior of **3**.

On the basis of this in silico superimposition, obtained over the 3D structures of **1** and limited to this set of functional diltiazem analogues, it could be hypothesized that one region is specific for the modulation of the vasorelaxant activity, one region is specific for the modulation of the negative inotropic activity, and a third region, composed of a phenyl ring and a polar area, is common to compounds endowed with both cardiac and vascular properties, as highlighted in Figure 10. These considerations agree to some extent with the classical structure−activity relationships (SAR) of structural analogues of **1**. The importance of the basic center in the *N*,*N*-dimethylaminoethyl side chain of **1** and the importance of its two aromatic rings about 7 Å apart are well-known. In particular, modifications to the aliphatic chain modulated

the vasorelaxant activity[30] whereas substituents on the condensed phenyl ring enhanced the potency.[31] A comprehensive analysis of the SARs of **1** and its structural and functional analogues is given in refs 7 and 32.

Conclusion

For the new cardiovascular LTCCs blocker 1-[(4-chlorophenyl)sulfonyl]-2-(2-thienyl)pyrrolidine (**3**), found by virtual screening, a comparison of experimental and calculated VCD spectra permitted the unambiguous assignment of the absolute configuration as *R*-(+)/*S*-(−), and a broad investigation of the antagonist activity of both enantiomers of **3** involving functional, electrophysiology, and binding studies. The functional profile on guinea pig was studied by assessing the negative inotropic and chronotropic action on left and right atria. The vasorelaxant activity was assessed on high K^+-depolarized aortic strips and ileum longitudinal smooth muscle. The effect on $I_{Ba(L)}$ recorded in rat vascular myocytes was assessed via the patch-clamp technique. The affinity to and the direct interaction with the cardiac LTCCs was verified using binding experiments carried out on rat cardiomyocytes with [^{3}H]diltiazem.

As a result of such a large analysis, stereoselective behavior for the negative inotropic activity and stereospecific behavior for the vasorelaxant activity were observed, whereas comparable binding and electrophysiological profiles were observed for the two enantiomers. While *R*-(+)-**3** was the more potent negative inotropic enantiomer, the vasorelaxant profile was exclusively assigned to *S*-(−)-**3**.

In conclusion, with the results presented here, compound **3** can be considered as a new and valid pharmacological tool to characterize the BTZ site in the cardiac α_1 subunit of the LTCC. Interestingly, all these data are in agreement with the in silico 3D-superimpositions obtained with the algorithm of the program FLAP specifically designed for ligand-based studies and used here for modeling some functional analogues of diltiazem. Combining this multidisciplinary research with the in silico procedure, the 3D orientations obtained led us to hypothesize relationships of molecular moieties to biological properties. In prospective, these results could pave the way to the design of new molecules as selective calcium modulators. Preliminary studies are currently in progress in this direction and will be published in due course.

Experimental Section

Purity of compounds was > 99%, as determined by HPLC (see below, section A).

A. Purity of Tested Compounds. Starting materials (±)-**3** and **4** were purchased from Maybridge Chemicals,[33] and compound **5** was from Key Organics Ltd.[34] HPLC-grade water and acetonitrile were purchased from Carlo Erba (Carlo Erba Reagents, Rodano, Italy). HPLC system consisted of a Waters 2695 (Waters, Milford, MA) chromatograph equipped with automatic injector and column heater and coupled with a model 996 PDA detector (Waters, Milford, MA). Thermo Finnigan LCQ Deca XP Plus ion trap mass spectrometer equipped with an ESI ion source was used for mass detection. Purity of compounds was checked by RP-HPLC using a Phenomenex Luna C18 column (250 mm × 4.6 mm i.d.). Gradient elution was obtained with solvents A (H_2O/ACN, 90/10) and B (ACN/H_2O, 90/10) starting from 60% B and reaching 100% B in 15 min at a flow rate of 1 mL/min. Eluents were 0.45 μm filtered before use. PDA data were acquired in the 200−400 nm range, and the 254 nm signal was extracted. Solutions of each sample in acetonitrile ($c = 10^{-5}$ M) were employed for MS flow injection analysis.

1-[(4-Chlorophenyl)sulfonyl]-2-(2-thienyl)pyrrolidine ((±)-3). ^{1}H NMR (400 MHz, CD_3OD) δ 1.76−2.10 (m, 4H), 3.38−3.46 (m, 1H), 3.50−3.60 (m, 1H), 5.17 (dd, 1H, J = 2.80 Hz, J = 6.86 Hz), 6.93 (dd, 1H, ^2J = 3.51 Hz, ^3J = 5.06 Hz), 6.97−7.00 (m, 1H), 7.26 (dd, 1H, ^2J = 1.25 Hz, ^3J = 5.06), 7.54−7.59 (m, 2H), 7.73−7.78 (m, 2H) ppm. HPLC: 254 nm, t_R = 12.39 min, purity > 99%. MS (ESI): m/z = 328 $[M + H]^+$.

1-[(4-Chlorophenyl)sulfonyl]-2-(methylthio)-1,4,5,6-tetrahydropyrimidine (4). ^{1}H NMR (400 MHz, CD_3OD) δ 1.80 (quin, 2H, ^3J = 5.90 Hz), 2.22 (s, 3H), 3.46 (t, 2H, ^3J = 5.90 Hz), 3.85 (t, 2H, ^3J = 5.90 Hz), 7.64 (d, 2H, J_{ortho} = 8.50 Hz), 7.97 (d, 2H, J_{ortho} = 8.50 Hz) ppm. HPLC: 254 nm, t_R = 10.05 min, purity > 99%. MS (ESI): m/z = 305 $[M + H]^+$.

***N*-Allyl-4-chloro-*N*-phenylbenzenesulfonamide (5).** ^{1}H NMR (400 MHz, CD_3OD) δ 4.26 (d, 2H, ^3J = 6.20 Hz), 5.06 (dd, 1H, ^2J = 1.0 Hz, ^3J = 11.2 Hz), 5.12 (dd, 1H, ^2J = 1.0 Hz, ^3J = 17.1 Hz), 5.70−5.82 (m, 1H), 7.05−7.10 (m, 2H), 7.28−7.35 (m,3H), 7.57 (d, 2H, J_{ortho} = 8.90 Hz), 7.59 (d, 2H, J_{ortho} = 8.90 Hz) ppm. HPLC: 254 nm, t_R = 13.09 min, purity > 99%. MS (ESI): m/z = 308 $[M + H]^+$.

B. Details for Enantiomers Separation and Absolute Configuration Determination. Experimental Data. The analytical HPLC resolution of (±)-**3** was performed on an analytical chromatograph equipped with a Rheodyne model 7725i 20 μL loop injector, a PU-1580-CO2 and PU-980 Jasco HPLC pumps, a UV detector Jasco-975, and a circular dichroism detector Jasco 995-CD. Chromatographic data were collected and processed using Borwin software (Jasco Europe, Italy). The chemical purity of (±)-**3** was checked on an analytical chromatograph equipped with a Rheodyne model 7725i 20 μL loop injector, a Waters 1525 HPLC pump, and a UV Waters 2487 detector. Chromatographic data were collected and processed using Empower2 (Waters, Milford, MA). The semipreparative HPLC resolution of (±)-**3** was performed on a Waters chromatograph (Waters Associates) equipped with a Rheodyne model 7012 500 μL loop injector and a UV SpectraMonitor 4100 and a refractive index Waters R401 detectors. The ECD spectra of (+)- and (−)-**3** in acetonitrile were recorded on a Jasco J710 spectropolarimeter. IR spectra of (+)-**3**, (−)-**3**, and (±)-**3** (potassium bromide dispersion) were recorded on a Jasco 430 FT-IR spectrometer. Specific rotations at 589 nm of (+)-**3** and (−)-**3** dissolved in acetonitrile were recorded on a Jasco P-1030 polarimeter.

Methods. All HPLC-grade solvents and reagents were purchased from Sigma-Aldrich, and the mobile phases were filtered before use over 0.45 μm filters. The chemical purity check of (±)-**3** was performed by gradient RP-HPLC using a C18 Luna Phenomenex column (250 mm × 4.6 mm i.d.) and gradient elution from (A) H_2O/ACN (90/10) and (B) ACN/H_2O (90/10) at a flow rate of 1 mL/min. The gradient elution started from A/B 40/60 (3 min hold) to B 100% in 15 min. The chromatographic profiles were acquired at 25 °C, using UV detection at 254 nm. The analytical HPLC resolution of (±)-**3** was carried out on a Chiralpak-IA column (250 mm × 4.6 mm i.d.) using hexane/isopropanol/dichloromethane, 85/10/5, as eluent, delivered at a flow rate of 1 mL/min. The column temperature was set at 25 °C. UV detection was carried out at 254 nm. The enantiomers of (±)-**3** were resolved by semipreparative HPLC using a Chiralpak-IA column (250 mm × 10 mm i.d.) with hexane/isopropanol/dichloromethane, 85/10/5, as eluent delivered at a flow rate of 4 mL/min. The column temperature was set at 25 °C. UV detection was carried out at 254 nm. Racemic **3** was dissolved in the mobile phase (c = 30.3 mg/mL), and for each run, an amount of 100 μL of solution, corresponding to 3 mg of racemic **3**, was injected.

Determination of Absolute Configuration. The experimental IR and VCD spectra of the enantiomers and racemate of **3** were measured using $CDCl_3$ solutions in cells of path lengths 236 and 546 μm using a Thermo Nicolet Nexus 670 FTIR instrument and a Bomem/BioTools ChiralIR Fourier transform VCD instrument. Conformational analysis of **3** was carried out using

the MMFF94 molecular mechanics force field and the SPARTAN 02 program.[35] Conformations obtained were reoptimized using DFT and the Gaussian 03 program.[36] Harmonic vibrational frequencies were then calculated for all conformations to verify their stability and to predict their relative free energies. Harmonic dipole and rotational strengths were simultaneously calculated, and IR and VCD spectra were then obtained using Lorentzian bandshapes ($\gamma = 4\ cm^{-1}$). Comparison of the DFT calculated VCD spectra for both enantiomers of **3** to the experimental VCD spectrum of (+)-**3** enables the absolute configuration of **3** to be reliably determined.[12]

C. Details for Functional Experiments. Functional Studies. The selected compounds were assayed on guinea pig left and right atria for negative inotropic and chronotropic action, respectively, while activity on vascular and nonvascular smooth muscle was assessed on high K^+-depolarized guinea pig aortic strips and ileum longitudinal smooth muscle. In particular, compounds were checked at increasing concentrations to evaluate the percent decrease of developed tension on isolated left atrium driven at 1 Hz (negative inotropic activity), the percent decrease in atrial rate on spontaneously beating right atrium (negative chronotropic activity), and the percent inhibition of calcium-induced contraction in 80 mM K^+-depolarized aortic strips (vasorelaxant activity) or ileum longitudinal smooth muscle (GPILSM relaxant activity).[3] The functional activity determined was expressed as efficacy and potency.

In Vitro Screening. Isolated Guinea Pig Left and Right Atria Preparations. Female guinea pigs (300−400 g) were sacrificed by cervical dislocation. After thoracotomy, the heart was immediately removed and washed by perfusion through the aorta with oxygenated Tyrode solution of the following composition (mM): NaCl, 136.9; KCl, 5.4; $CaCl_2$, 2.5; $MgCl_2$, 1.0; $NaH_2PO_4 \cdot H_2O$, 0.4; $NaHCO_3$, 11.9; glucose, 5.5. The physiological salt solution (PSS) was buffered to pH 7.4 by saturation with 95% O_2−5% CO_2 gas, and the temperature was maintained at 37 °C. Isolated guinea pig heart preparations were used, i.e., spontaneously beating right atria and left atria driven at 1 Hz. For each preparation, the entire left and right atria were dissected from the ventricles, cleaned of excess tissue, and hung vertically in a 15 mL organ bath containing the PSS continuously bubbled with 95% O_2−5% CO_2 gas at 35 °C, pH 7.4. The contractile activity was recorded isometrically by means of force transducer (FT 0.3, Grass Instruments, Quincy, MA) using Power Lab software (ADInstruments Pty Ltd., Castle Hill, Australia). The left atria were stimulated by rectangular pulses of 0.6−0.8 ms duration and about 50% threshold voltage through two platinum contact electrodes in the lower holding clamp (Grass S88 stimulator, Quincy, MA). The right atrium was in spontaneous activity. After the tissue was beating for several minutes, a length−tension curve was determined, and the muscle length was fixed at that eliciting 90% of maximum contractile force observed at the optimal length. A stabilization period of 45−60 min was allowed before the atria were used to test compounds. During the equilibration period, the bathing solution was changed every 15 min and the threshold voltage was ascertained for the left atria. Atrial muscle preparations were used to examine the inotropic and chronotropic activity of the compounds (0.1, 0.5, 1, 5, 10, 50, and 100 μM) first dissolved in DMSO and then diluted with PSS. According to this procedure, the concentration of DMSO in the bath solution never exceeded 0.3%, a concentration that did not produce significant inotropic and chronotropic effects. During the construction of cumulative concentration−response curves, the next higher concentration of the compound was added only after the response to the previous one had reached a steady state.

Guinea Pig Aortic Strips and Ileum Longitudinal Smooth Muscle (GPILSM). The thoracic aorta and ileum were removed and placed in Tyrode solution (PSS) of the following composition (mM): NaCl, 118; KCl, 4.75; $CaCl_2$, 2.54; $MgSO_4$, 1.20; KH_2PO_4, 1.19; $NaHCO_3$, 25; glucose, 11. This solution was equilibrated with 95% O_2−5% CO_2 gas at pH 7.4. The vessel was cleaned of connective tissue. Two helicoidal strips (10 mm × 1 mm) were cut from each aorta beginning from the end most proximal to the heart. Vascular strips were then tied with surgical thread (6−0) and suspended in a jacketed organ bath (15 mL) containing aerated PSS at 35 °C. Aortic strips were secured at one end to Plexiglas hooks and connected via the surgical thread to a force displacement transducer (FT 0.3, Grass Instruments Corporation, Quincy, MA) for monitoring changes in isometric contraction. Aortic strips were subjected to a resting tension of 1 g. The intestine was excised above the ileocecal junction and the mesenteric tissue removed. The longitudinal smooth muscle was gently separated from the ileum portion, and segments of 2 cm length were mounted at one end to Plexiglas hooks under a resting tension of 300−400 mg. Strips were secured at the other end to a force displacement transducer (FT 0.3, Grass Instruments Corporation, Quincy, MA) for monitoring changes in isometric contraction and washed every 20 min with fresh PSS for 1 h. After the equilibration period, guinea pig aortic strips were contracted by washing in PSS containing 80 mM KCl (equimolar substitution of K^+ for Na^+). When the contraction reached a plateau (about 45 min), various concentrations of the compounds (0.1, 0.5, 1, 5, 10, 50, 100, and 500 μM) were added cumulatively to the bath, allowing for any relaxation to obtain an equilibrated level of force. Addition of the drug vehicle (DMSO for all compounds) had no appreciable effect on K^+-induced contraction.

Statistical Analysis. Data were analyzed using Student's *t* test and are presented as the mean ± SEM.[10] Since the drugs were added in cumulative manner, significant differences ($P < 0.05$) between control and experimental values at each concentration were indicated by asterisks. The potency of drugs defined as EC_{50}, EC_{30}, and IC_{50} was evaluated from log concentration−response curves (Probit analysis using Litchfield and Wilcoxon[10] or GraphPad Prism software[37]) in the appropriate pharmacological preparations.

D. Details for Binding Experiments. Cardiomyocytes Isolation. This investigation conforms to the Guide for the Care and Use of Laboratory Animals published by the U.S. National Institutes of Health (NIH Publication No. 85-23, revised 1996), and the animal protocols used were reviewed and approved by the Animal Care and Ethics Committee of the Università degli Studi di Siena, Italy. Single cardiac myocytes (CM) were isolated from male Wistar rats (body weight 376 ± 12 g, $n = 19$, Charles River Italia, Calco, Italy), injected with 500 U heparin/100 g body weight, i.p., anesthetized with a mixture of Ketavet (30 mg kg^{-1} ketamine; Gellini, Italy) and Xilor (8 mg kg^{-1} xylazine; Bayer, Germany), decapitated, and bled.[38] After thoracotomy, the heart was rapidly removed, mounted on a micro-Langendorff apparatus, and perfused for 20 min at 37 °C with a nominally Ca^{2+}-free solution (low Ca^{2+} solution, LCS) of the following composition (mM): NaCl, 120; KCl, 10; HEPES, 10; glucose, 10; $MgCl_2$, 1.2; KH_2PO_4, 1.2; sodium pyruvate, 5; taurine, 20; pH 7.2, equilibrated with 95% O_2−5% CO_2. The solution was then quickly changed to LCS complemented with 0.9 mg/mL collagenase type I (Sigma Chimica, Milan, Italy), 0.05 mg/mL dispase I (Roche Gmbh, Penzbeg, Germany), and 1.5 mg/mL bovine serum albumin acid-free (Sigma Chimica, Milan, Italy) for 10−15 min. When the heart was soft, perfusion was stopped and the tissue was chopped into small pieces and gently stirred in fresh LCS at room temperature. The cardiomyocytes that appeared in the supernatant were purified by centrifugation (5 min at 800*g*) and frozen at −80 °C until use. Pooled cells, derived from at least two animals, were used for each binding experiment. Protein concentrations were estimated by the method of Bradford[39] with BSA as standard.

[^{3}H]Diltiazem Binding Assays. [^{3}H]Diltiazem binding assays were performed according to earlier methods[40,41] with some modifications. Aliquots of thawed rat CM (200 μg) were incubated with ligands in 50 mM Tris buffer (pH 7.4) at 25 °C for

90 min in a final volume of 0.2 mL. In homologous competition curves, [^{3}H]diltiazem (specific activity 85.5 Ci/mmol) was present at 20 nM in tubes containing increasing concentrations of unlabeled diltiazem (5 nM to 100 μM) and at 0.1−20 nM in tubes without unlabeled ligand. In heterologous competition curves, a fixed amount of the tracer (5 nM) was displaced by increasing concentrations of several unlabeled ligands (0.1 nM to 100 μM). The incubation was terminated by a rapid filtration on Whatman GF/B glass fiber filters (presoaked for at least 1 h in 0.5% polyethyleneimmine) and washed three times with 3 mL of ice-cold wash buffer. The filters were then placed in scintillation vials. An amount of 5 mL of scintillation liquid was added and the radioactivity measured in a LS5000CE β-counter (Beckman Instruments, Palo Alto, CA). Nonspecific binding was defined by means of 100 μM unlabeled diltiazem. All the experiments were always run in triplicate.

Data Analysis. All the data, presented as mean ± SEM, were reported by plotting specific binding (% of control) versus log of the inhibitor concentration (M) and fitted with a nonlinear (sigmoidal) analysis.

E. Details for Electrophysiological Experiments. Tail Main Artery Dissection. This investigation conforms to the Guide for the Care and Use of Laboratory Animals published by the U.S. National Institutes of Health (NIH Publication No. 85-23, revised 1996), and the animal protocols used were reviewed and approved by the Animal Care and Ethics Committee of the Università degli Studi di Siena, Italy (31.01.2006). Male Wistar rats (300−400 g, Charles River Italia, Calco, Italy) were anesthetized with a mixture of Ketavet (30 mg kg^{-1} ketamine; Gellini, Italy) and Xilor (8 mg kg^{-1} xylazine; Bayer, Germany), decapitated, and bled. Tail was immediately removed, cleaned of skin, and placed in 0.1 mM Ca^{2+} external solution (see below for composition). The tail main artery was dissected free, removing the connective tissue.

Cell Isolation Procedure for $I_{Ba(L)}$ Recordings. Smooth muscle cells were freshly isolated from the tail main artery incubated at 37 °C in 2 mL of 0.1 mM Ca^{2+} external solution (see below) containing 1 mg/mL collagenase (type XI), 1 mg/mL soybean trypsin inhibitor, and 1 mg/mL bovine serum albumin and gently bubbled with a 95% O_2−5% CO_2 gas mixture, as previously described.[42] Cells exhibited an ellipsoid form (10−15 μm in width, 35−55 μm in length) and were continuously superfused with recording solution containing 0.1 mM Ca^{2+} using a peristaltic pump (LKB 2132, Bromma, Sweden), at a flow rate of 400 μL min^{-1}.

Whole-Cell Patch-Clamp Recordings. The conventional whole-cell patch-clamp method[43] was employed to voltage-clamp smooth muscle cells. Recording electrodes were pulled from borosilicate glass capillaries (WPI, Berlin, Germany) and fire-polished to obtain a pipet resistance of 2−5 MΩ when filled with internal solution (see below). A low-noise, high-performance Axopatch 200B (Molecular Devices Corporation, CA) patch-clamp amplifier driven by a personal computer (pClamp 9.2.1.8 software; Molecular Devices Corporation, CA) in conjunction with an A/D, D/A board (DigiData 1200 A/B series interface, Molecular Devices Corporation, CA) was used to generate and apply voltage pulses to the clamped cells and record the corresponding membrane currents. At the beginning of each experiment, the junction potential between the pipette and bath solutions was electronically adjusted to zero. Cell break-in was accomplished by gentle suction at a holding potential (V_h) of −50 mV. Then V_h was set to −80 mV. Micropipette seals had to be GΩ in nature with leak currents less than 0.25 pA mV^{-1}. Current signals, after compensation for whole-cell capacitance and series resistance (70−80%), were low-pass-filtered at 1 kHz and digitized at 3 kHz prior to being stored on the computer hard disk. Electrophysiological responses were tested at room temperature (20−22 °C) only in those cells that were phase dense.

$I_{Ba(L)}$ Recordings. Cells used in this study expressed LTCCs but not T-type Ca^{2+} channels.[44] $I_{Ba(L)}$ was always recorded in 5 mM Ba^{2+}-containing recording solution. Current was elicited with 250 ms clamp pulses (0.067 Hz) to 0 mV from a V_h of −80 mV until a stable current response was achieved (usually 6−9 min after the whole-cell configuration had been obtained). $I_{Ba(L)}$ did not run down during the following 20−30 min under these conditions.[44] K^+ currents were blocked with 30 mM tetraethylammonium in the external solution and Cs^+ in the internal solution (see below). Current values were corrected for leakage using 10 μM nifedipine, which was proved to block completely $I_{Ba(L)}$. Following control measurements, each cell was exposed to cumulative concentration of a drug by flushing through the experimental chamber recording solution containing the drug. Compounds (±)-**3**, *S*-(−)-**3**, and *R*-(+)-**3**, dissolved directly in DMSO, were diluted at least 1000 times prior to use. The resulting concentrations of DMSO (below 0.1%, v/v) failed to alter the response of the preparations. Acquisition and analysis of data were accomplished by using pClamp 9.2.1.8 software and GraphPad Prism version 5.01.[33] Data are reported as the mean ± SEM. *n* is the number of cells analyzed (indicated in parentheses), isolated from at least three animals. The IC_{50} values were calculated from log concentration−response curves.

Solutions for $I_{Ba(L)}$ Recordings. The Ca^{2+}-free external solution contained the following (mM): NaCl, 110; KCl, 5.6; HEPES, 10; glucose, 20; taurine, 20; $MgCl_2$, 1.2; sodium pyruvate, 5; pH 7.4. The Ca^{2+}-free recording solution contained the following (in mM): NaCl, 130; KCl, 5.6; HEPES, 10; glucose, 20; $MgCl_2$, 1.2; sodium pyruvate, 5; pH 7.4. The internal solution (pCa 8.4) consisted of the following (mM): CsCl, 100; HEPES, 10; EGTA, 11; $MgCl_2$, 2; $CaCl_2$, 1; Na-pyruvate, 5; succinic acid, 5; oxalacetic acid, 5; Na_2-ATP, 3; phosphocreatine, 5; pH was adjusted to 7.4 with CsOH. The osmolarity of recording solution (320 mosmol) and that of the internal solution (290 mosmol) were checked with an osmometer (Osmostat OM 6020, Menarini Diagnostics, Italy).

F. Computational methods. Details for the 3D-Superimposition Procedure. The program FLAP[24] (fingerprint for ligands and proteins) was originally conceived as a fast algorithm for performing virtual screening by means of a fingerprint-type description of both ligands and protein binding sites. It was designed to describe molecules and protein structures in terms of a common reference framework. This framework can be built from information obtained from the active site of the protein of interest, in which case the resulting study is called structure-based study, or from ligands that are known to be active for a certain biological target, in which case the resulting study is called a ligand-based study. In ligand-based virtual screening, compounds from virtual libraries are ranked according to their similarity toward a given reference molecule, called a template.[24] Given the 3D structure of a molecule, with the GRID force field[25] the interaction energy between the molecule and a probe is calculated at different points in space. As a result, one has the so-called molecular interaction fields (MIF): the hydrophobic and hydrogen bonding interactions of the molecule with a virtual receptor are schematized by the probes and encoded into energy values assigned to the nodes of a grid built around each molecule. MIF are of central importance in the execution of the FLAP algorithm since, given two molecules, their MIF are used by FLAP to align one over the other. The first step of the FLAP procedure is the creation of a database: all the molecules imported will be referred to as ligand molecules. The ligand molecules are subjected to a fast conformational analysis, a reasonable number of conformations are generated, and each conformer is individually treated (in this application, up to 100 conformations were generated by FLAP). Some representative fields are extracted from the MIF of the individual elements entered and stored in the database. Then a molecular template is imported, the corresponding MIF are calculated with the program GRID, and again some representative fields are selected from the MIF. The pairwise similarity is calculated on the basis of MIF superimposition which, in turn, is obtained by

combining quadruplets of hotspots that could be either molecular atoms or points from the MIF. The first case was used: FLAP classifies all the heavy atoms of ligand molecules as hydrophobic, hydrogen bond donating or accepting, and positively or negatively charged. Then FLAP describes each molecule as a set of quadruplets, derived by combining all the hotspots, four by four, in an exhaustive way. Each quadruplet is defined by the character of its composing hotspots, by their six interatomic distances, measured in angstroms and binned in 1 Å intervals, and by an additional flag for the chirality of the quadruplet. The huge information obtained is then documented in a fingerprint mode where the absence or presence of all quadruplets corresponds to 0 or 1, respectively. For computational reasons, only present quadruplets are stored in such a way that facilitates further searches and uses. The information obtained for the template molecule is stored in a virtual bit string, making future computations much easier and quicker to complete and compare. The next step in the FLAP process would be finding the matches of the four hotspots of the individual ligands to those of the template. When four hotspots of the ligand molecule are found to fit over four hotspots of the template framework, a potentially favorable superimposition has been detected. Of course, the process is iterative, and it will continue until all the template quadruplets are combined in all possible ways with all ligand quadruplets. Each time, a score associated with the two molecules and their common quadruplet of hotspots quantifies the overlap of the two MIF: a score is assigned to the superimposition in order to evaluate its "goodness" of MIF-overlapping, using the MIF of the two molecules produced with the GRID probes DRY and OH2. At the end of the process, only the best superimposition of each ligand to each template is memorized. Some details of the FLAP calculations are briefly listed: (1) the tolerance between pairwise atoms (from template and ligand molecules) was set to 1 Å. (2) The conformers are produced by FLAP on-the-fly with a routine that randomly modifies the molecule and adds a new conformation to the set only when it differs from the ones already existing. The difference is calculated by using rmsd (root-mean-square deviation) criteria, using 0.1 as threshold for considering two conformations enough diverse to be treated individually. In this way, the FLAP conformational sampling guarantees an adequate treatment of molecular flexibility in order to span as much as possible the conformational space. For the template **1** the conformational analysis was carried out on-the-fly producing 10 different conformations and repeating for each conformation the entire procedure described, whereas up to 100 conformers were generated for each ligand molecule, and the best results obtained among these was the result assigned to the compound. (3) GRID probes DRY and OH2 was used to describe the template and each ligand molecule. In addition, the GRID probe H is used for describing the molecular shape. (4) The molecular atoms were used as hotspots. (5) The level of speed was set to 75%.

Acknowledgment. Financial support was provided by grants from Universities of Bologna, Perugia, Siena, and Roma and from Ministero dell'Istruzione, dell'Università e della Ricerca (Grants PRIN 2005034305_001, PRIN 20078J9L2A_005, and FIRB RBPR05NWWC_003). We are also grateful for financial support from the U.S. National Science Foundation (to P.J.S., Grants CHE-0209957 and CHE-0614577). We also thank the USC High Performance Computing and Communication (HPCC) facility for computer time.

Supporting Information Available: The B3PW91/TZ2P structures and geometries of the conformers **a**−**g** of *R*-(+)-**3** (with room-temperature equilibrium populations of >2%) together with their DFT calculated frequencies, dipole strengths, and rotational strengths. This material is available free of charge via the Internet at http://pubs.acs.org.

References

(1) McGregor, M. J.; Luo, Z.; Jiang, X. Virtual Screening in Drug Discovery. In *Drug Discovery Research. New Frontiers in the Post-Genomic Era*; Huang, Z., Ed.; Wiley-VCH: Weinheim, Germany, 2007; pp 63−88.
(2) Budriesi, R.; Cosimelli, B.; Ioan, P.; Lanza, C. Z.; Spinelli, D.; Chiarini, A. Cardiovascular Characterization of [1,4]Thiazino[3,4-*c*]-[1,2,4]oxadiazol-1-one-derivatives: Selective Myocardial Calcium Channel Modulators. *J. Med. Chem.* **2002**, *45*, 3475–3481.
(3) Budriesi, R.; Carosati, E.; Chiarini, A.; Cosimelli, B.; Cruciani, G.; Ioan, P.; Spinelli, D.; Spisani, R. A New Class of Selective Myocardial Calcium Channel Modulators. 2. The Role of the Acetal Chain in Oxadiazol-3-one Derivatives. *J. Med. Chem.* **2005**, *48*, 2445–2456.
(4) Carosati, E.; Cruciani, G.; Chiarini, A.; Budriesi, R.; Ioan, P.; Spisani, R.; Spinelli, D.; Cosimelli, B.; Fusi, F.; Frosini, M.; Matucci, R.; Gasparrini, F.; Ciogli, A.; Stephens, P. J.; Devlin, F. J. New Calcium Channel Antagonists Discovered by a Multidisciplinary Approach. *J. Med. Chem.* **2006**, *49*, 5206–5216.
(5) Maron, B. J. Hypertrophic Cardiomyopathy: A Systematic Review. *JAMA, J. Am. Med. Assoc.* **2002**, *287*, 1308–1320.
(6) Varon, J. Treatment of Acute Severe Hypertension: Current and Newer Agents. *Drugs* **2008**, *68*, 283–97.
(7) Budriesi, R.; Cosimelli, B.; Ioan, P.; Carosati, E.; Ugenti, M. P.; Spisani, R. Diltiazem Analogues: The Last Ten Years on Structure Activity Relationships. *Curr. Med. Chem.* **2007**, *14*, 279–287.
(8) Carosati, E.; Budriesi, R.; Ioan, P.; Ugenti, M. P.; Frosini, M.; Fusi, F.; Corda, G.; Cosimelli, B.; Spinelli, D.; Chiarini, A.; Cruciani, G. Discovery of Novel and Cardioselective Diltiazem-like Calcium Channel Blockers via Virtual Screening. *J. Med. Chem.* **2008**, *51*, 5552–5565.
(9) Agrawal, Y. K.; Bhatt, H. G.; Raval, H. G.; Oza, P. M.; Gogoi, P. J. Chirality, a New Era of Therapeutics. *Mini-Rew Med. Chem.* **2007**, *7*, 451–460.
(10) Tallarida, R. J.; Murray, R. B. *Manual of Pharmacologic Calculations with Computer Programs*, 2nd ed.; Springer-Verlag: New York, 1987.
(11) Garcia, M. L.; King, V. F.; Siegl, P. K.; Reuben, J. P.; Kaczorowski, G. J. Binding of Ca^{2+} Entry Blockers to Cardiac Sarcolemmal Membrane Vesicles. Characterization of Diltiazem-Binding Sites and Their Interaction with Dihydropyridine and Aralkylamine Receptors. *J. Biol. Chem.* **1986**, *261*, 8146–8157.
(12) Stephens, P. J.; Devlin, F. J.; Pan, J. J. The Determination of the Absolute Configuration of Chiral Molecules Using Vibrational Circular Dichroism (VCD) Spectroscopy. *Chirality* **2008**, *20*, 643–663.
(13) Stephens, P. J.; Pan, J. J.; Devlin, F. J.; Cheeseman, J. R. Determination of the Absolute Configurations of Natural Products Using TDDFT Optical Rotation Calculations: The Iridoid Oruwacin. *J. Nat. Prod.* **2008**, *71*, 285–288.
(14) Krohn, K.; Gehle, D.; Dey, S. K.; Nahar, N.; Mosihuzzaman, M.; Sultana, N.; Sohrab, M. H.; Stephens, P. J.; Pan, J. J.; Sasse, F. Prismatomerin, a New Iridoid from *Prismatomeris tetrandra*. Structure Elucidation, Determination of Absolute Configuration and Cytotoxicity. *J. Nat. Prod.* **2007**, *70*, 1339–1343.
(15) Stephens, P. J.; Pan, J. J.; Krohn, K. Determination of the Absolute Configurations of Pharmacological Natural Products via Density Functional Theory Calculations of Vibrational Circular Dichroism: The New Cytotoxic Iridoid Prismatomerin. *J. Org. Chem.* **2007**, *72*, 7641–7649.
(16) Stephens, P. J.; Devlin, F. J.; Schürch, S.; Hulliger, J. Determination of the Absolute Configuration of Chiral Molecules via Density Functional Theory Calculations of Vibrational Circular Dichroism and Optical Rotation: The Chiral Alkane D_3-anti-trans-anti-trans-anti-trans-Perhydrotriphenylene. *Theor. Chem. Acc.* **2008**, *119*, 19–28.
(17) Stephens, P. J.; Devlin, F. J.; Villani, C.; Gasparrini, F.; Mortera, S. L. Determination of the Absolute Configurations of Chiral Organometallic Complexes via Density Functional Theory Calculations of Their Vibrational Circular Dichroism Spectra: The Chiral Chromium Tricarbonyl Complex of *N*-Pivaloyl-tetrahydroquinoline. *Inorg. Chim. Acta* **2008**, *361*, 987–999.
(18) Stephens, P. J.; Pan, J. J.; Devlin, F. J.; Urbanová, M.; Julinek, O.; Hájiček, J. Determination of the Absolute Configurations of Natural Products via Density Functional Theory Calculations of Vibrational Circular Dichroism, Electronic Circular Dichroism and Optical Rotation: The Isoschizozygane Alkaloids Isoschizogaline and Isoschizogamine. *Chirality* **2008**, *20*, 454–470.

(19) Drabowicz, J.; Zajac, A.; Lyzwa, P.; Stephens, P. J.; Pan, J. J.; Devlin, F. J. Determination of the Absolute Configurations of Isotopically Chiral Molecules Using Vibrational Circular Dichroism (VCD) Spectroscopy: The Isotopically Chiral Sulfoxide Perdeuteriophenyl-phenyl-sulfoxide. *Tetrahedron: Asymmetry* **2008**, *19*, 288–294.
(20) Figadère, B.; Devlin, F. J.; Millar, J. G.; Stephens, P. J. Determination of the Absolute Configuration of the Sex Pheromone of the Obscure Mealybug by Vibrational Circular Dichroism Analysis. *Chem. Commun.* **2008**, *9*, 1106–1108.
(21) Stephens, P. J.; Devlin, F. J.; Gasparrini, F.; Ciogli, A.; Spinelli, D.; Cosimelli, B. Determination of the Absolute Configuration of a Chiral Oxadiazol-3-one Calcium Channel Blocker, Resolved Using Chiral Chromatography, via Concerted Density Functional Theory Calculations of Its Vibrational Circular Dichroism, Electronic Circular Dichroism, and Optical Rotation. *J. Org. Chem.* **2007**, *72*, 4707–4715.
(22) Zhang, T.; Kientzy, C.; Franco, P.; Ohnishi, A.; Kagamihara, Y.; Kurosawa, H. Solvent Versatility of Immobilized 3,5-Dimethylphenylcarbamate of Amylose in Enantiomeric Separations by HPLC. *J. Chromatogr., A* **2005**, *1075*, 65–75.
(23) Cerè, V.; Peri, F.; Pollicino, S.; Ricci, A.; Devlin, F. J.; Stephens, P. J.; Gasparrini, F.; Rompietti, R.; Villani, C. Synthesis, Chromatographic Separation, Vibrational Circular Dichroism Spectroscopy, and ab Initio DFT Studies of Chiral Thiepane Tetraol Derivatives. *J. Org. Chem.* **2005**, *70*, 664–669.
(24) Baroni, M.; Cruciani, G.; Sciabola, S.; Perruccio, F.; Mason, J. S. A Common Reference Framework for Analyzing/Comparing Proteins and Ligands. Fingerprints for Ligands and Proteins (FLAP): Theory and Application. *J. Chem. Inf. Model.* **2007**, *47*, 279–294.
(25) (a) Goodford, P. J. A Computational Procedure for Determining Energetically Favorable Binding Sites on Biologically Important Macromolecules. *J. Med. Chem.* **1985**, *28*, 849–857. (b) Carosati, E.; Sciabola, S.; Cruciani, G. Hydrogen Bonding Interactions of Covalently Bonded Fluorine Atoms: From Crystallographic Data to a New Angular Function in the GRID Force Field. *J. Med. Chem.* **2004**, *47*, 5114–5125. (c) *GRID*, version 22 for Linux; Molecular Discovery Ltd. (215 Marsh Road, HA5 5NE Pinner, Middlesex, U.K.); http://www.moldiscovery.com.
(26) DeLano, W. L. *The PyMOL Molecular Graphics System*; DeLano Scientific LLC: Palo Alto, CA, 2008; http://www.pymol.org.
(27) Tikhonov, D. B.; Zhorov, B. S. Benzothiazepines in L-Type Calcium Channel: Insights from Molecular Modelling. *J. Biol. Chem.* **2008**, *283*, 17594–17604.
(28) Hering, S.; Savchenko, A.; Strübing, C.; Lakitsch, M.; Striessnig, J. Extracellular Localization of the Benzothiazepine Binding Domain of L-Type Ca^{2+} Channels. *Mol. Pharmacol.* **1993**, *43*, 820–826.
(29) Dilmac, N.; Hilliard, N.; Hockerman, G. H. Molecular Determinants of Ca^{2+} Potentiation of Diltiazem Block and Ca^{2+}-Dependent Inactivation in the Pore Region of $Ca_v1.2$. *Mol. Pharmacol.* **2003**, *64*, 491–501.
(30) (a) Inoue, H.; Konda, M.; Hashiyama, T.; Otsuka, H.; Watanabe, A.; Gaino, M.; Takahashi, K.; Date, T.; Okamura, K.; Takeda, M.; Narita, H.; Murata, S.; Odawara, A.; Sasaki, H.; Nagao, T. Synthesis and Biological Evaluation of Alkyl, Alkoxy, Alkylthio, or Amino-Substituted 2,3-Dihydro-1,5-benzothiazepin-4(5*H*)-ones. *Chem. Pharm. Bull.* **1997**, *45*, 1008–1026. (b) Inoue, H.; Konda, M.; Hashiyama, T.; Otsuka, H.; Takahashi, K.; Gaino, M.; Date, T.; Aoe, K.; Takeda, M.; Murata, S.; Narita, H.; Nagao, T. Synthesis of Halogen-Substituted 1,5-Benzothiazepine Derivatives and Their Vasodilating and Hypotensive Activities. *J. Med. Chem.* **1991**, *34*, 675–687.
(31) Schleifer, K. J.; Tot, E. Molecular Modeling Study of Diltiazem Mimics at L-Type Calcium Channels. *Pharm. Res.* **1999**, *16*, 1506–1513.
(32) Budriesi, R.; Ioan, P.; Carosati, E.; Cruciani, G.; Zhorov, B. S.; Chiarini, A. Ligands of Diltiazem Binding Site: An Overview of Some Chemotypes. *Mini-Rev. Med. Chem.*, in press.
(33) http://www.maybridge.com.
(34) http://www.keyorganics.ltd.uk.
(35) *Spartan 02*; Wavefunction Inc.: Irvine, CA.
(36) Frisch, M. J.; Trucks, G. W.; Schlegel, H. B.; Scuseria, G. E.; Robb, M. A.; Cheeseman, J. R.; Montgomery, J. A., Jr.; Vreven, T.; Kudin, K. N.; Burant, J. C.; Millam, J. M.; Iyengar, S. S.; Tomasi, J.; Barone, V.; Mennucci, B.; Cossi, M.; Scalmani, G.; Rega, N.; Petersson, G. A.; Nakatsuji, H.; Hada, M.; Ehara, M.; Toyota, K.; Fukuda, R.; Hasegawa, J.; Ishida, M.; Nakajima, T.; Honda, Y.; Kitao, O.; Nakai, H.; Klene, M.; Li, X.; Knox, J. E.; Hratchian, H. P.; Cross, J. B.; Adamo, C.; Jaramillo, J.; Gomperts, R.; Stratmann, R. E.; Yazyev, O.; Austin, A. J.; Cammi, R.; Pomelli, C.; Ochterski, J. W.; Ayala, P. Y.; Morokuma, K.; Voth, G. A.; Salvador, P.; Dannenberg, J. J.; Zakrzewski, V. G.; Dapprich, S.; Daniels, A. D.; Strain, M. C.; Farkas, O.; Malick, D. K.; Rabuck, A. D.; Raghavachari, K.; Foresman, J. B.; Ortiz, J. V.; Cui, Q.; Baboul, A. G.; Clifford, S.; Cioslowski, J.; Stefanov, B. B.; Liu, G.; Liashenko, A.; Piskorz, P.; Komaromi, I.; Martin, R. L.; Fox, D. J. Keith, T.; Al-Laham, M. A.; Peng, C. Y.; Nanayakkara, A.; Challacombe, M.; Gill, P. M. W.; Johnson, B.; Chen, W.; Wong, M. W.; Gonzalez, C.; Pople, J. A. *Gaussian 03*; Gaussian, Inc.: Pittsburgh, PA, 2004.
(37) *GraphPad Prism*, versions 3.02, 4.03, and 5.01; GraphPad Software Inc.: La Jolla, CA; http://www.graphpad.com.
(38) Matucci, R.; Ottaviani, M. F.; Barbieri, M.; Cerbai, E.; Mugelli, A. Protective Effect of Darodipine, a Calcium Antagonist, on Rat Cardiomyocytes against Oxygen Radical-Mediated Injury. *Br. J. Pharmacol.* **1997**, *122*, 1353–1360.
(39) Bradford, M. M. A Rapid and Sensitive Method for the Quantitation of Microgram Quantities of Protein Utilizing the Principle of Protein−Dye Binding. *Anal. Biochem.* **1976**, *72*, 248–254.
(40) Wei, X. Y.; Rutledge, A.; Triggle, D. J. Voltage-Dependent Binding of 1,4-Dihydropyridine Ca^{2+} Channel Antagonists and Activators in Cultured Neonatal Rat Ventricular Myocytes. *Mol. Pharmacol.* **1989**, *35*, 541–552.
(41) Zobrist, R. H.; Mecca, T. E. [^{3}H]TA-3090, a Selective Benzothiazepine-Type Calcium Channel Receptor Antagonist: In Vitro Characterization. *J. Pharmacol. Exp. Ther.* **1990**, *253*, 461–465.
(42) Fusi, F.; Saponara, S.; Gagov, H.; Sgaragli, G. P. 2,5-Di-*t*-butyl-1,4-benzohydroquinone (BHQ) Inhibits Vascular L-Type Ca^{2+} Channel via Superoxide Anion Generation. *Br. J. Pharmacol.* **2001**, *133*, 988–996.
(43) Hamill, O. P.; Marty, A.; Neher, E.; Sakmann, B.; Sigworth, F. J. Improved Patch-Clamp Techniques for High-Resolution Current Recording from Cells and Cell-Free Membrane Patches. *Pflugers Arch.* **1981**, *391*, 85–100.
(44) Petkov, G. V.; Fusi, F.; Saponara, S.; Gagov, H.; Sgaragli, G. P.; Boev, K. K. Characterization of plasma membrane calcium currents in freshly isolated smooth muscle cells from rat tail main artery. *Acta Physiol. Scand.* **2001**, *173*, 257–265.